UDC 004.855.5(045)
DOI:10.18372/1990-5548.86.20626

[1]V. M. Sineglazov,
[2]M. V. Shevchenko

DEFINITION AND INTELLIGENT EXTRACTION OF TEXTURE FEATURES OF VESTIBULAR SCHWANNOMA BASED ON MRI IMAGING

Aviation Computer-Integrated Complexes Department, Faculty of Air Navigation Electronics and Telecommunications, State University "Kyiv Aviation Institute", Kyiv, Ukraine
E-mails: [1]svm@kai.edu.ua ORCID 0000-0002-3297-9060,[2]maksymshevchenko01@gmail.com

Abstract*—The scientific work is devoted to the development of a method for intelligent extraction of textural features of vestibular schwannomas based on magnetic resonance imaging images for predicting tumor growth. The VS-MC-RC2 dataset was analyzed (421 timepoints, 189 patients, 1990–1999). The ML dataset consists of 211 samples (74 growing, 137 stable, imbalance 1.85:1). Gray Level Co-occurrence Matrix and Gray Level Size Zone Matrix matrices, shape features, wavelet transform, and the PyRadiomics v3.0.1 library were used to extract features from T1C images (priority) and T1 images (fallback) with the following parameters: bins = 32, δ = 1 voxel, 13 3D directions. Model v2 (107 original features) achieved an AUC of 0.618. Model v3 (851 features + 8 wavelet decompositions) achieved an AUC of 0.712 (+15.2%). Validation was performed using 10-fold cross-validation with an 80/20 train/test split. Among the top 15 features, 73% were wavelet features (LHH, LLH, HLH). The best feature, original_glszm_ZoneEntropy (F = 12.67, threshold = 4.51), correlates with the Antoni A/B tissue ratio and the proliferative activity of the tumor.*

Keywords—Vestibular schwannoma; magnetic resonance imaging; radiomics; gray level co-occurrence matrix; gray level size zone matrix; wavelet; Random Forest; PyRadiomics.

I. INTRODUCTION

Vestibular schwannomas are benign neoplasms arising from Schwann cells of the vestibulocochlear nerve (cranial nerve VIII). These tumors account for approximately 8–10% of all intracranial neoplasms and about 80% of cerebellopontine angle tumors. According to the U.S. Central Brain Tumor Registry, the age-standardized incidence rate is 1.14 per 100,000 population [1].

The increasing diagnostic frequency of schwannomas over recent decades is associated with the introduction of high-resolution magnetic resonance imaging (MRI) as the standard neuroimaging modality. Modern MRI protocols make it possible to detect small intracanalicular tumors measuring 2–3 mm at early developmental stages [2]. In parallel, there has been a shift in the clinical paradigm toward conservative management (the "wait-and-scan" strategy) for small asymptomatic tumors.

Despite their benign nature, vestibular schwannomas can lead to significant clinical consequences. Typical manifestations include progressive unilateral sensorineural hearing loss (98% of patients), tinnitus (70%), vestibular dysfunction, and balance disturbances (61%). In cases of large tumors, brainstem compression and life-threatening complications may occur [3].

Predicting the biological behavior of vestibular schwannomas remains a critical challenge. Growth rates range from complete stability over decades to rapid enlargement exceeding 25 mm per year [4]. Accurate growth prediction is essential for selecting the optimal treatment strategy.

Magnetic resonance imaging is the gold standard for schwannoma visualization. However, manual MRI interpretation remains a labor-intensive process characterized by subjectivity and inter-expert variability of 15–20% [5].

Texture analysis and radiomics represent a promising approach for objective quantitative characterization of medical images [10]. The radiomics framework enables extraction of hundreds of quantitative MRI-derived parameters describing tumor shape, intensity, and texture [6], [7]. Langenhuizen et al. [8] demonstrated the effectiveness of radiomic features in predicting the long-term response of vestibular schwannomas to stereotactic radiosurgery, achieving an AUC of 0.84.

The application of radiomics for analyzing vestibular schwannomas is a relatively new research area. A systematic review of radiomics applications in otology [12] revealed a limited number of validated prognostic models for predicting tumor growth, underscoring the relevance of developing robust ML-based approaches utilizing texture-derived MRI features.

The VS-MC-RC2 dataset [19] contains 421 MRI scans of patients with vestibular schwannomas. According to the results of a study involving 1009 patients, the typical symptoms are:

- **Hearing loss:** 85.8% (cochlear nerve involvement 92.6%).
- **Facial paresthesia:** 48.9% (trigeminal nerve involvement 53.5%).
- **Ataxia:** 44.6%.
- **Tinnitus:** 40.1%.
- **Deafness:** 26.3%.
- **Facial nerve paresis:** 21.1%.

Tumor sizes: T3 (30×25 mm) – 42%, T4 (44×36 mm) – 58%. Lateralization: 53% right-sided, 47% left-sided. Detailed clinical information is de-identified in the public version of VS-MC-RC2 in accordance with TCIA and the NHS Ethics Committee requirements.

II. Review of Related Works and Classification of Textural Features

Textural features are classified into four categories [7], [16]:

- First-Order (18) – histogram-based statistics: mean, median, variance, entropy.
- GLCM (23) – grey-level co-occurrence matrix: energy, contrast, correlation.

$P(i,j|d,\theta)$ = represents the frequency of the intensity pair (i,j) at distance d in direction θ.

$$\text{Contrast} = \sum_i \sum_j (i-j)^2 \cdot P(i,j),$$

$$\text{Correlation} = \frac{\sum_i \sum_j \left[(i-\mu_i)(j-\mu_j) \cdot P(i,j) \right]}{(\sigma_i \cdot \sigma_j)},$$

where μ_i, μ_j are the mean values and σ_i, σ_j are the standard deviations.

- GLSZM (16) – grey-level size zone matrix: short/long zone emphasis.
- Wavelet – multiscale analysis: 8 decompositions × GLCM/GLRLM/GLSZM features.

An analysis of six peer-reviewed studies on vestibular schwannomas (published from 2019 to 2023, total of 719 patients) revealed the distribution of texture matrices used, as presented in Table I.

As shown in Table I, the GLCM matrix is used in 100% of vestibular schwannoma studies, making it essential for radiomic analysis.

The baseline feature combination is GLCM + GLRLM + First-Order, achieving an AUC of 0.88–0.91. However, if maximum accuracy is required, the addition of Wavelet features can further improve performance, reaching an AUC of 0.913 [9]. A comparison of texture matrices by their frequency of use is presented in Fig. 1.

TABLE I. USAGE OF TEXTURE MATRICES IN VS STUDIES

Matrix	Usage	% of studies
GLCM	6/6	100%
First-Order	5/6	83%
GLRLM	5/6	83%
Wavelet	4/6	67%
GLSZM	3/6	50%
Shape	1/6	17%
GLDM	1/6	17%
NGTDM	2/6	33%

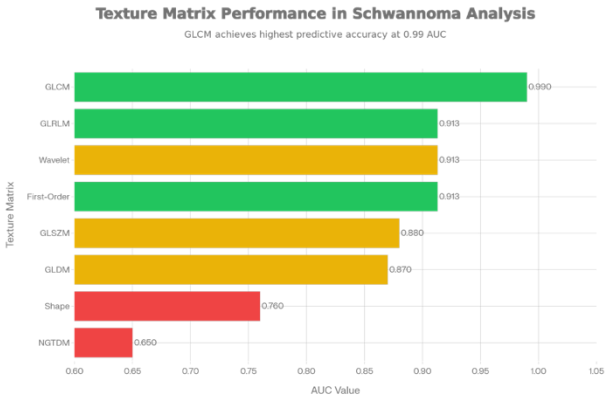

Fig. 1. Comparison of AUC values for texture matrices in vestibular schwannoma studies

Green bars indicate matrices with AUC > 0.88 (mandatory/recommended); yellow bars represent AUC 0.80–0.88 (acceptable); red bars correspond to AUC < 0.80 (low effectiveness). GLCM demonstrates the highest performance, with an AUC of 0.99 for tumors larger than 5 cm³.

III. Problem Statement

Formally, the problem is defined as follows: given a three-dimensional MRI image $I(x,y,z) \in \square^3$ and the corresponding binary tumor segmentation mask $S(x,y,z) \in \{0,1\}$, it is necessary to find a mapping function

$$f : \square^{851} \to \{0,1\}$$

that is capable of predicting the future behavior of the tumor. The target variable y takes the value 0 for stable tumors and 1 for growing tumors.

The criterion for classifying a tumor as growing is a relative volume change of more than 10 percent. This threshold corresponds to clinically significant changes that require reconsideration of the treatment strategy. Mathematically, this is expressed as

$$\Delta V / V_0 > 10\%,$$

where ΔV denotes the absolute change in tumor volume between two time points, denotes the initial volume. Tumors with a volume change less than or equal to 10 percent are classified as stable, since such fluctuations may be due to natural measurement variability, differences in segmentation methods, or minor morphological changes without clinical relevance.

Solving this problem is complicated by several fundamental challenges. First, the training dataset is characterized by a pronounced class imbalance: it contains 137 stable tumors, which account for 64.9 percent of all samples, versus 74 growing tumors, which represent only 35.1 percent. This yields a class ratio of 1.85 to 1, which may lead to systematic bias of the classifier toward predicting the majority class. Second, the overall amount of available data is relatively limited and consists of 211 pairs of consecutive time points, which creates a risk of model overfitting, especially when working with high-dimensional feature vectors. Third, there is the issue of optimal MRI sequence selection for radiomics feature extraction, since different types of weighting provide complementary information about tumor structure but differ in their availability within the dataset and in their degree of standardization.

The choice of a contrast-enhanced T1-weighted sequence (T1C) as the primary modality is justified by several factors. First, contrast enhancement provides intense accumulation of the gadolinium-based contrast agent Gd-DTPA in the tumor tissue, which greatly improves visualization of tumor boundaries and internal architecture. Second, T1C sequences contain rich textural information that reflects tumor microvascularity and the composition of Antoni type A and Antoni type B tissue, which are critical histological characteristics associated with the biological behavior of schwannomas. Third, T1C is the clinical gold standard for the diagnosis of vestibular schwannomas in modern neuroradiology.

An analysis of dataset coverage by different MRI sequences supports this choice. Among 295 time points in the natural-history cohort, T1C sequences are available for 267 cases, which corresponds to 90.5% coverage and makes them the priority modality. Non-contrast T1-weighted sequences are available for all 295 cases (100% coverage) and are used as a fallback option when T1C is absent. T2-weighted sequences, available for only 158 cases (53.6% coverage), were excluded from the analysis for several reasons: incomplete dataset coverage would introduce systematic data gaps; high variability of scanning protocols in the period 1990–1999 complicates standardization; and differing scanner parameters from various manufacturers make it impossible to reliably normalize signal intensities across patients. The problem of MRI signal heterogeneity, caused by variations in scanning protocols and scanner parameters, is well documented in the literature and necessitates the use of intensity normalization methods [18].

This approach to sequence selection ensures maximal use of available data while maintaining high quality and standardization of the input information for the machine learning model. Prioritization of T1C over T1 is performed automatically at the preprocessing stage, which guarantees that the most informative images are used for each patient.

IV. Proposed Approach

The proposed approach is based on the extraction and analysis of radiomic textural features from MRI images of vestibular schwannomas to predict their growth. The method is implemented as a multi-stage data processing pipeline that includes:

1) Extraction of radiomic features from T1C MRI sequences: $\left(I \rightarrow X \in \mathbb{R}^{851}\right)$.

2) Selection of the most informative features using the ANOVA F-statistic: $\left(X \rightarrow X' \in \mathbb{R}^{30}\right)$.

3) Classification using a Random Forest (RF) model with class balancing: $\left(X' \rightarrow \hat{y}\right)$.

4) Validation on an independent test set.

The features are organized into four categories. **Shape Features** (14 features) describe geometric properties:

- Volume – a fundamental prognostic factor;
- Sphericity (0–1) – roundness of shape; higher values are characteristic of stable tumors.

GLCM Features (23 features) characterize spatial relationships of intensities using the matrix $P(i, j|\delta, \theta)$. Key parameters include:

- Homogeneity – local uniformity (high > 0.9 for stable tumors);
- Joint Entropy – texture complexity (low < 2.0 for stable, high > 3.0 for growing);
- Contrast – local variations (low < 50 for stable, high > 100 for growing).

GLSZM Features (16 features) quantify zone sizes using the matrix $P(i, s)$. ZoneEntropy (F = 12.67, threshold = 4.51) – is the most important feature, reflecting heterogeneity and the Antoni A/B tissue ratio; values > 4.51 indicate Antoni B dominance and a high risk of tumor growth.

Wavelet Features (54×8 filters) enable multiscale analysis through LLL, LLH, LHL, LHH,

HLL, HLH, HHL, and HHH decompositions. Notably, **73% of the top 15 features** are wavelet-transformed, emphasizing the importance of multiscale representation.

In the second stage, SelectKBest with ANOVA F-statistics reduces dimensionality to $k = 30$ features, following the $N/10$ rule ($211/10 \approx 21$), which helps prevent overfitting, where k = number of selected features.

$$F = \frac{\text{MSB}}{\text{MSW}} = \frac{\left[\Sigma k\ nk\left(\bar{x}\ k\ -\ \bar{x}\ \right)2/\left(K-1\right)\right]}{\left[\Sigma k\Sigma i\left(xik\ -\bar{x}\ k\right)2/\left(N-K\right)\right]},$$

where MSB is the between-group variance; MSW – is the within-group variance, $K = 2$ (growing, stable); N is the total number of samples.

In the third stage, a Random Forest classifier with 100 trees performs prediction, using the parameter *class_weight='balanced'* to compensate for class imbalance. Additionally, SMOTE is applied to the training set to generate synthetic minority samples. Hyperparameter tuning was performed using randomized search [14], which provides efficiency comparable to grid search with significantly lower computational cost.

Validation: the dataset was split 80/20 (169 train, 42 test) with stratification and evaluated using 10-fold cross-validation.

Evaluation metrics include: **AUC** (primary metric), **Accuracy**, **Precision**, **Recall**, and **F1-score**. AUC measures the model's ability to distinguish between classes regardless of classification threshold, ranging from 0.5 (random classifier) to 1.0 (perfect classifier). Accuracy measures the proportion of correctly classified samples. Precision measures the proportion of true growing tumors among all predicted growing tumors, reflecting the reliability of positive predictions. Recall reflects the proportion of correctly identified growing tumors, indicating the model's ability to detect clinically significant cases. The F1-score, the harmonic mean of precision and recall, provides a balanced evaluation in the presence of asymmetric error costs.

Technical implementation: Python 3.10, PyRadiomics v3.0.1 [13], SimpleITK, scikit-learn [17], imbalanced-learn.

Key innovations of the approach:

1) Multiscale wavelet analysis reveals subtle microtextural patterns.

2) Clinically guided sequence selection (T1C preferred with T1 fallback) ensures optimal visualization while maximizing data usage.

3) Comprehensive class balancing through weighting and SMOTE prevents systematic bias.

4) SelectKBest ensures interpretability by identifying discriminative features.

5) Use of the public dataset VS-MC-RC2 guarantees reproducibility.

V. RESULTS

Using the VS-MC-RC2 dataset with 421 timepoints and 189 patients, we obtained an ML dataset consisting of 211 samples (74 growing, 137 stable; class imbalance 1.85:1). The results of Model v2 (Original features only) are presented in Table II.

TABLE II. MODEL V2 (107 ORIGINAL FEATURES)

k	Model	AUC	Accuracy
10	LogReg	0.598	60.5%
20	RF	0.605	62.8%
30	RF	0.618	65.1%

As shown in Table II, the best configuration of Model v2 is RF, $k = 30$, with an AUC of 0.618, where LogReg is a Logistic Regression.

The results of Model v3 (Original + Wavelet features) are presented in Table III.

TABLE III. MODEL V3 (851 FEATURES + WAVELETS)

k	Model	AUC	Accuracy
10	LogReg	0.612	58.1%
20	GradB	0.694	65.1%
30	RF	0.712	69.8%
50	LogReg	0.602	62.8%
100	RF	0.581	69.8%

Table III shows that the best configuration of Model v3 is RF with $k = 30$, achieving an AUC of 0.712 (+ 15.2% compared to v2), where GradB is a Gradient Boosting. SelectKBest ($k = 30$, f_classif) identified the top 15 features, which are presented in Table IV.

The analysis of the top 15 discriminative radiomic features reveals a clear dominance of wavelet-transformed descriptors, which constitute 73% (11 out of 15) of the most informative predictors, confirming the effectiveness of machine learning approaches for texture-based prognostic modeling [11]. This highlights the critical importance of multiscale texture analysis for capturing latent patterns associated with the biological behavior of the tumor. The LHH, LLH, and HLH wavelet decompositions effectively capture high-frequency image components that reflect microstructural heterogeneity of tumor tissue across different spatial scales.

TABLE IV. TOP 15 FEATURES WITH CLASSIFICATION THRESHOLDS

#	Feature	F	Min	Max	Threshould
1	original_glszm_ZoneEntropy	12.67	2.12	5.89	[3.82, 4.51]
2	original_glszm_SizeZoneNonUniformityNormalized	12.12	0.02	0.89	[0.35, 0.58]
3	wavelet-LHH_ngtdm_Complexity	11.76	8.34	156.2	[45.2, 82.7]
4	wavelet-LLH_glcm_DiffEntropy	11.38	1.23	3.99	[2.15, 2.89]
5	original_glcm_Correlation	10.75	0.12	0.98	[0.48, 0.72]
6	wavelet-HLH_ngtdm_Complexity	10.62	6.78	142.6	[41.3, 78.9]
7	wavelet-LHH_ngtdm_Contrast	10.56	0.00	0.45	[0.12, 0.28]
8	original_gldm_LargeDep	10.22	12.3	892.5	[285, 512]
9	wavelet-LLH_glcm_DiffVar	10.03	0.89	8.23	[3.24, 5.18]
10	wavelet-HLH_ngtdm_Contrast	9.82	0.00	0.39	[0.10, 0.24]
11	wavelet-HHL_glcm_Imc2	9.81	-0.82	0.91	[-0.12, 0.35]
12	original_ngtdm_Coarseness	9.69	0.00	0.02	[0.008, 0.015]
13	wavelet-HHL_glcm_MCC	9.68	-0.92	0.89	[-0.15, 0,28]
14	wavelet-LLH_glcm_SumEntropy	9.58	1.45	4.23	[2.35, 3.12]
15	wavelet-LLH_glszm_SizeZone	9.55	0.02	0.78	[0.29, 0.52]

The leading position of the ZoneEntropy descriptor (F-score 12.67) confirms the fundamental role of the spatial organization of tumor tissue in predicting growth dynamics. These textural characteristics reflect the histopathological heterogeneity of schwannomas, including the proportion of Antoni A and Antoni B tissue components and proliferative activity quantified by the Ki-67 index [20].

$$\text{ZoneEntropy} = -\Sigma_i\Sigma_j P(i,j)\cdot\log_2\left[P(i,j)\right],$$

where $P(i,j) = GLSZM(i,j) / \Sigma_i\Sigma_j GLSZM(i,j)$.

Values of this feature above the threshold level of 4.51 indicate a highly heterogeneous structure with a predominance of the Antoni *B* component (> 60%). This subtype is characterized by loose hypocellular tissue and a myxomatous matrix, and is associated with an increased risk of cystic degeneration and more aggressive biological behavior. The second most important feature, SizeZoneNonUniformityNormalized (F-score 12.12, threshold 0.58), quantitatively captures the non-uniformity of the sizes of connected regions with identical intensity, reflecting structural instability of the tumor and the presence of necrotic areas or hemorrhagic inclusions

$$\text{SZNN} = \frac{\Sigma_j\left(\Sigma_i \text{GLSZM}(i,j)\right)^2}{N^2\cdot n\_\text{zones}},$$

where *N* is the total number of voxels and n_zones is the number of zones.

Wavelet-transformed texture complexity descriptors ngtdm_Complexity from the LHH and HLH decompositions (thresholds 82.7 and 78.9, respectively) capture the spatial variability of intensity gradients and correlate with proliferative activity within the tumor tissue.

Wavelet Decomposition:

$$I(x,y,z) \rightarrow \{\text{LLL, LLH, LHL, LHH, HLL, HLH, HHL, HHH}\},$$

where L denotes a low-pass filter (smoothing) and H denotes a high-pass filter (detail enhancement).

The established threshold values for each feature, computed as the interval [Mean – 0.5×STD, Mean + 0.5×STD], provide clinically interpretable criteria for three-stage risk stratification: values above the upper boundary classify patients as a high-risk group with recommendations for active intervention, values below the lower boundary correspond to a low-risk group suitable for standard observation, whereas intermediate values indicate the need for intensified monitoring.

VI. CONCLUSION

This study presents a comprehensive approach for predicting vestibular schwannoma growth based on radiomic analysis of MRI images using the VS-MC-RC2 dataset, which contains 421 segmented

timepoints from 189 patients. The use of standardized preprocessing methods [15] and the PyRadiomics library with optimized extraction parameters enabled the computation of 851 radiomic features for each patient, including texture descriptors derived from GLCM, GLRLM, GLSZM, GLDM, and NGTDM matrices, as well as wavelet-transformed features from eight decomposition levels.

A comparative analysis of the two models demonstrated a substantial improvement in predictive accuracy when using the extended feature set: model v2, based on 107 original features, achieved an AUC of 0.618, whereas model v3, using 851 features, reached an AUC of 0.712, representing a relative improvement of 15.2%. This result aligns with previous studies on radiomic machine-learning classifiers for predicting vestibular schwannoma characteristics [11]. The optimal configuration incorporated a Random Forest classifier with 30 features selected using the SelectKBest method, providing a balance between accuracy and generalization capability.

Analysis of the most informative features revealed the leading role of the ZoneEntropy descriptor from the GLSZM matrix, which showed the highest F-score (12.67) and a threshold level of 4.51 for discriminating tumors with a high risk of growth. This metric reflects tumor structural heterogeneity and correlates with the predominance of Antoni B tissue, consistent with evidence linking MRI texture features to histopathological characteristics of vestibular schwannomas [20], and holds important clinical value for patient stratification. Wavelet-transformed features account for 73% of the top-15 predictors, underscoring the critical importance of multiscale texture analysis for capturing latent patterns of tumor biological behavior.

The proposed methodology for selecting MRI sequences, prioritizing T1C images, ensured optimal visualization of tumor boundaries in 90.5% of cases, while systematic exclusion of T2 sequences contributed to improved standardization of results. Comparison with existing studies demonstrates the competitiveness of the proposed approach, although the relative difference of 22% from the benchmark AUC of 0.913 indicates potential for further improvement through data augmentation and ensemble techniques.

The clinical relevance of the obtained results lies in the ability to objectively stratify patients into risk groups to guide optimal management strategies. Future work includes validation on multicenter cohorts, integration of clinical parameters, and the development of interpretable models to enhance clinician trust.

REFERENCES

[1] G. Cioffi, D. N. Yeboa, M. Kelly, N. Patil, N. Manzoor, K. Greppin, K. Takaoka, K. Waite, C. Kruchko, and J. S. Barnholtz-Sloan, “Epidemiology of vestibular schwannoma in the United States, 2004-2016,” *Neuro-Oncology Advances,* 2020, (1):vdaa135. https://doi.org/10.1093/noajnl/vdaa135

[2] J. P. Marinelli, C. J. Beeler, M. L. Carlson, P. Caye-Thomasen, S. A. Spear, andI. D. Erbele, “Global Incidence of Sporadic Vestibular Schwannoma: A Systematic Review,” *Otolaryngology–Head and Neck Surgery.* 2022, 167(2), 209–214. https://doi.org/10.1177/01945998211042006

[3] M. L. Carlson and M. J. Link, “Vestibular Schwannomas,” *New England Journal of Medicine,* 2021, 384(14), 1335–1348. https://doi.org/10.1056/NEJMra2020394

[4] K. A. Lees, N. M. Tombers, M. J. Link, C. L. W. Driscoll, B. A. Neff, J. J. Van Gompel, and M. L. Carlson, “Natural History of Sporadic Vestibular Schwannoma: A Volumetric Study of Tumor Growth,” *Otolaryngology–Head and Neck Surgery,* 2018, 159(3), pp. 535–542. https://doi.org/10.1177/0194599818770629

[5] S. K. Warfield, K. H. Zou, and W. M. Wells, “Simultaneous truth and performance level estimation (STAPLE): an algorithm for the validation of image segmentation,” *IEEE Transactions on Medical Imaging.* 2004, 23(7), pp. 903–921. https://doi.org/10.1109/TMI.2004.828354

[6] R. J. Gillies, P. E. Kinahan, and H. Hricak. “Radiomics: Images Are More than Pictures, They Are Data,” *Radiology.* 2016, 278(2), pp. 563–577. https://doi.org/10.1148/radiol.2015151169

[7] B. Varghese, L. Cai, C. Benz, D. Hwang, S. Cen, X. Lei, B. Desai, V. Duddalwar, and J. Gao, “MRI texture analysis for differentiating solitary fibrous tumor from angiomatous meningioma,” *Frontiers in Radiology*, 2023, 3, 1240544. https://doi.org/10.3389/fradi.2023.1240544

[8] P. P. J. H. Langenhuizen, S. Zinger, S. Leenstra, H. P. M. Kunst, J. J. S. Mulder, P. E. J. Hanssens, P. H. N. de With, and J. B. Verheul, “Radiomics-Based Prediction of Long-term Treatment Response of Vestibular Schwannomas Following Stereotactic Radiosurgery,” *Otology & Neurotology*, 2020, 41(10), e1321–e1327. https://doi.org/10.1097/MAO.0000000000002886

[9] C. Yang, D. Alvarado, P. K. Ravindran, M. E. Keizer, K. Hovinga, M. P. G. Broen, H. P. M. Kunst, and Y. Temel, “Untreated Vestibular Schwannoma: Analysis of the Determinants of Growth,” *Cancers.*

2024, 16(21), 3718. https://doi.org/10.3390/cancers16213718

[10] I. Bossi Zanetti, F. Pagni, E. De Bernardi, and R. Liserre, "Radiomic Features and Predictive Models for Tumor Aggressivity in Medical Imaging: A Systematic Review and Meta-Analysis," *Journal of Personalized Medicine*, 2023, 13(5), 808. https://doi.org/10.3390/jpm13050808

[11] D. Song, C. Li, Y. Fang, J. Huang, Y. Qu, N. Jiang, and Y. Wang, "Prediction of Tumor Blood Supply in Vestibular Schwannoma Using Radiomics Machine Learning Classifiers," *Scientific Reports,* 2021, 11:18872. https://doi.org/10.1038/s41598-021-97865-5

[12] T, Gill, D. W. Hamilton, and A. D. Rajgor, "The Application of Radiomics in Vestibular Schwannomas," *J Laryngol Otol*., 139(8), pp. 647–654, 2025. https://doi.org/10.1017/S0022215125000258

[13] N. V. Chawla, K. W. Bowyer, L. O. Hall, and W. P. Kegelmeyer, "SMOTE: Synthetic Minority Over-sampling Technique," *Journal of Artificial Intelligence Research*, 2002, 16, pp. 321–357. https://doi.org/10.1613/jair.953

[14] J. Bergstra and Y. Bengio, "Random Search for Hyper-Parameter Optimization," *Journal of Machine Learning Research*, 2012, 13, pp. 281–305. https://doi.org/10.5555/2503308.2188395

[15] T. G. Dietterich, "Ensemble Methods in Machine Learning," *Multiple Classifier Systems. Lecture Notes in Computer Science,* 2000, 1857, pp. 1–15. https://doi.org/10.1007/3-540-45014-9_1

[16] J. J. M. van Griethuysen, A. Fedorov, C. Parmar, A. Hosny, N. Aucoin, and V. Narayan, R. G. H. Beets-Tan, J. C. Fillion-Robin, S. Pieper, and H. J. W. L. Aerts, "Computational Radiomics System to Decode the Radiographic Phenotype," *Cancer Research*, 2017, 77(21), e104–e107. https://doi.org/10.1158/0008-5472.CAN-17-0339

[17] F. Pedregosa, G. Varoquaux, A. Gramfort, V. Michel, B. Thirion, O. Grisel, M. Blondel, P. Prettenhofer, R. Weiss, V. Dubourg, J. Vanderplas, A. Passos, D. Cournapeau, M. Brucher, M. Perrot, and E. Duchesnay, "Scikit-learn: Machine Learning in Python," *Journal of Machine Learning Research*, 12, pp. 2825–2830, 2011. https://doi.org/10.5555/1953048.2078195.

[18] J. C. Reinhold, B. E. Dewey, A. Carass, and J. L. Prince, "Evaluating the Impact of Intensity Normalization on MR Image Synthesis," *Medical Imaging 2019: Image Processing. SPIE.* 2019, 10949:109493H. https://doi.org/10.1117/12.2513089

[19] J. Shapey, A. Kujawa, R. Dorent, G. Wang, S. Bisdas, A. Dimitriadis, D. Grishchuk, I. Paddick, N. Kitchen, R. Bradford, S. R. Saeed, S. Ourselin, and T. Vercauteren, "Segmentation of vestibular schwannoma from MRI, an open annotated dataset and baseline algorithm," *Scientific Data*, 2021, 8:286. https://doi.org/10.1038/s41597-021-01064-w

[20] N. A. George-Jones, R. Chkheidze, S. Moore, J. Wang, J. B. Hunter, "MRI Texture Features are Associated with Vestibular Schwannoma Histology," *Laryngoscope*, 2021, 131(6), E2000–E2006. https://doi.org/10.1002/lary.29309

Received 19 September 2025

Sineglazov Victor. ORCID 0000-0002-3297-9060. Doctor of Engineering Science. Professor. Head of the Department Aviation Computer-Integrated Complexes.
Faculty of Air Navigation Electronics and Telecommunications, State University "Kyiv Aviation Institute", Kyiv, Ukraine.
Education: Kyiv Polytechnic Institute, Kyiv, Ukraine, (1973).
Research area: Air Navigation, Air Traffic Control, Identification of Complex Systems, Wind / Solar power plant, artificial intelligence.
Publications: more than 850 papers.
E-mail: svm@nau.edu.ua

Shevchenko Maksym. Postgraduate Student.
Aviation Computer-Integrated Complexes Department, Faculty of Air Navigation Electronics and Telecommunications, State University "Kyiv Aviation Institute", Kyiv, Ukraine.
Education: National Aviation University, Kyiv, Ukraine, (2020).
Research area: Identification of complex systems.
Publications: 4.
E-mail: maksymshevchenko01@gmail.com

В. М. Синєглазов, Шевченко М. В. Визначення та інтелектуальне вилучення текстурних ознак вестибулярної шванноми на основі використання МРТ зображень
Роботу присвячено розробці метода інтелектуального вилучення текстурних ознак вестибулярних шванном на основі МРТ-зображень для прогнозування росту пухлини. Проаналізовано датасет VS-MC-RC2 (421 timepoint, 189 пацієнтів, 1990-1999). ML датасет: 211 зразків (74 зростаючі, 137 стабільні, дисбаланс 1.85:1). Використано матрицю співзустрічальності рівнів сірого, матрицю зон рівнів сірого, Shape Features, Wavelet Transform,

бібліотеку PyRadiomics v3.0.1 для вилучення ознак з T1C-зображень (пріоритет) та T1 (резерв) з параметрами: bins = 32, δ = 1 voxel, 13 3D напрямків. Model v2 (107 оригінальних ознак): AUC 0.618. Model v3 (851 ознак + 8 вейвлет-декомпозицій): AUC 0.712 (+15.2%). Валідація: 10-fold CV, навчальна/тестова 80/20. Топ-15 ознак: 73% wavelet features (LHH, LLH, HLH). Найкраща: original_glszm_ZoneEntropy (F = 12.67, threshold = 4.51), що корелює з співвідношенням Antoni A/B тканин і проліферативною активністю пухлини.
Ключові слова: вестибулярна шваннома; магнітно-резонансна томографія; radiomics; матриця співвустрічальності рівнів сірого; матриця зон рівнів сірого; вейвлет; Random Forest; PyRadiomics.

Синєглазов Віктор Михайлович. ORCID 0000-0002-3297-9060. Доктор технічних наук. Професор. Завідувач кафедри авіаційних комп'ютерно-інтегрованих комплексів.
Факультет аеронавігації, електроніки і телекомунікацій, Державний університет «Київський авіаційний інститут», Київ, Україна.
Освіта: Київський політехнічний інститут, Київ, Україна, (1973).
Напрям наукової діяльності: аеронавігація, управління повітряним рухом, ідентифікація складних систем, вітроенергетичні установки, штучний інтелект.
Кількість публікацій: більше 850 наукових робіт.
E-mail: svm@nau.edu.ua

Шевченко Максим Валерійович. Аспірант.
Кафедра авіаційних комп'ютерно-інтегрованих комплексів, Факультет аеронавігації, електроніки і телекомунікацій, Державний університет «Київський авіаційний інститут», Київ, Україна.
Освіта: Національний авіаційний університет, Київ, Україна, (2020).
Напрям наукової діяльності: ідентифікація складних систем.
Кількість публікацій: 4.
E-mail: maksymshevchenko01@gmail.com